Methodology to design LCL filter for a DC-DC boost converter with Zero-Voltage-Switching

Etienne BOULAUD, Thierry MEYNARD, Jose MANEIRO
University of Toulouse, CNRS, Alstom

ABSTRACT - This paper presents an analytical methodology for designing the LCL input filter of a converter for fuel cell applications. Fuel cell railway systems are powerful and must supply the traction system for several decades. Industrial concerns focus on fuel cell lifetime, and the power converter must support higher currents than previously. To ensure optimal performance and longevity, the current ripple in the fuel cell must be minimized, which stresses the usual tradeoff between inductor size, switching frequency, and efficiency. This tradeoff formulation changes significantly when a first-order input filter is replaced with a third-order input filter: the ripple in the fuel cell benefits from the increased order, and the switching frequency can be increased if the filter is designed to allow Zero Voltage Switching (ZVS) due to the high current ripple at the filter output. For SiC devices, turn-on losses are higher than turn-off losses, so ZVS provides a significant reduction in switching energies, enabling a much higher switching frequency.

Index Terms—Mosfet SiC, current ripple, Fuel Cell, losses

1. INTRODUCTION

Several tests and studies have shown the impact of high-frequency current ripple on fuel cell aging [1]. This constraint, originating from suppliers, should be a constant value derived from their own aging tests at a constant average current with triangular or sinusoidal ripple.
Due to the characteristics of fuel cells, high power demand results in voltage reduction. At zero current, our fuel cell voltage can reach around 500V and drop to 300V at maximum power. During a mission profile, fuel cells are primarily used to provide a constant or slowly varying average power. Therefore, for lifetime considerations, we only account for maximum power with low voltage, as other functional points in the range are only reached during transition phases. This corresponds to the average power demand required to supply traction and auxiliary systems.
Peak power demand during braking or acceleration is provided by a battery system directly connected to the traction system, as shown in Fig. 1. For railway systems, we can consider a DC-link on the battery side with a voltage around 1000V.

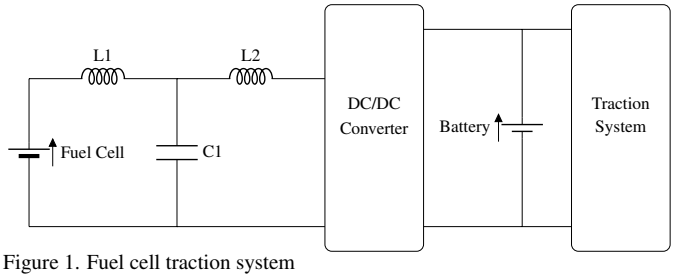

Figure 1. Fuel cell traction system

2. DC/DC ARCHITECTURE

2.1. Power semi-conductor devices

Frequency is a key aspect of the design when using small passive components. The latest generation of SiC MOSFETs allows switching our average current of around 400A at frequencies exceeding 10kHz. This high power density is achieved through thermal dissipation optimizations, based on the well-known chip losses and characteristics [2].

SiC device suppliers are focusing on the development of 1200V devices due to the demand from the electric automobile industry. They produce highly efficient devices with packaging that is well-suited to our cooling requirements. This voltage rating is suitable for batteries up to 800V [3], but railway systems require larger battery systems around 1000V.

2.2. Converter architecture

Several architectures can utilize 1200V devices in a 1000V application. For this study, a 3-level flying capacitor configuration is considered (Fig. 2). The methodology for designing the LCL filter described in this paper is applicable to other multi-level architectures with any number of levels.

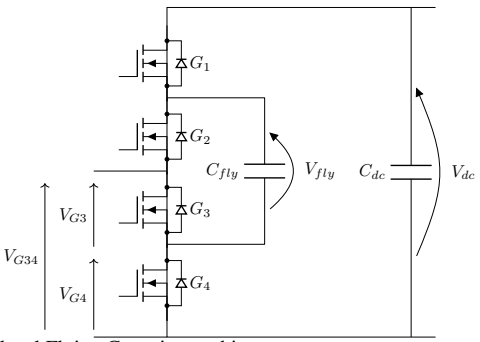

Figure 2. 3 level Flying Capacitor architecture

On the DC side, there is a filtering capacitor C_{dc} used to absorb the current chopped by G_1 and achieve a voltage with low ripple. A flying capacitor C_{fly} is added between switches to create a flying voltage source. In steady state, the flying voltage can be regulated to any value between $0V$ and V_{dc} with proper control, but a good approach is to set $V_{fly} = V_{dc}/2$. This value allows each switch to operate at $V_{dc}/2$ instead of V_{dc}.

A primary assumption is that the ripple voltage on V_{fly} and V_{dc} is negligible compared to the average voltage. Due to the high current, the capacitor value will be determined by the RMS current rather than its ripple. In practice, capacitors in parallel will be needed for thermal considerations, and the value will be higher than required for ripple considerations.

2.3. *Switching command*

The control signals of G_1 and G_2 are complementary to those of G_4 and G_3, respectively, to avoid short circuits with the capacitors.

The voltage gain between the fuel cell and the battery is defined as $G = V_{bat}/V_{fc}$. Consequently, the average duty cycle applied to the switches is defined as $\alpha = (G-1)/G$. A balanced way to operate the converter is to maintain the same frequency and the same duty cycle applied to G_3 and G_4, with a half-period delay between them. This ensures good current balancing through the flying capacitor in steady state.

3. LCL FILTER DESIGN

LCL filters are typically used in AC grids with connected converters [4]. They attenuate high-frequency current harmonics while preserving the fundamental frequency. However, LCL filters can also be applied to DC-DC applications. The simplest way to design them is to assume that the third-order filter will significantly attenuate current harmonics. This assumption allows for considering simple waveforms on passive components: square voltage on the converter side, triangular current in the inductance near the converter, and sinusoidal current through the inductor farther from the converter. This approach facilitates the quick study of ripple voltage or current [5].

3.1. *Input command*

This paper presents a more accurate method for designing LCL filters using Fourier series (1). Due to the periodicity in steady state and symmetries, it is possible to use Fourier series to describe $G_{1,2,3,4}$:

$$G_i(t) = \overline{G_i} + \sum_{n=1}^{+\infty} G_{in}\cos(n\omega t - \varphi_{in}) \tag{1}$$

The mean value depends on the duty cycle:

$$\overline{G} = \begin{Bmatrix} \overline{G_1} \\ \overline{G_2} \\ \overline{G_3} \\ \overline{G_4} \end{Bmatrix} = \begin{Bmatrix} 1-\alpha \\ 1-\alpha \\ \alpha \\ \alpha \end{Bmatrix} \tag{2}$$

The Fourier coefficients and phase depend on the square signal:

$$G_n = \begin{Bmatrix} G_{1n} \\ G_{2n} \\ G_{3n} \\ G_{4n} \end{Bmatrix} = \begin{Bmatrix} \frac{2\sin(n(1-\alpha)\pi)}{n\pi} \\ \frac{2\sin(n(1-\alpha)\pi)}{n\pi} \\ \frac{2\sin(n\alpha\pi)}{n\pi} \\ \frac{2\sin(n\alpha\pi)}{n\pi} \end{Bmatrix} \tag{3}$$

$$\varphi_n = \begin{Bmatrix} \varphi_{1n} \\ \varphi_{2n} \\ \varphi_{3n} \\ \varphi_{4n} \end{Bmatrix} = \begin{Bmatrix} 0 \\ n\pi \\ 0 \\ n\pi \end{Bmatrix} \tag{4}$$

The switch voltages V_{G3} and V_{G4} represent the capacitor voltages and are complementary to the switching states of V_{G1} and V_{G2}. It is possible to describe the input filter voltage V_{G34} with the following expression:

$$\begin{aligned} V_{G34}(t) = \overline{V_{fc}} + \overline{V_{fly}} \sum_{n=1}^{+\infty} G_{2n}\cos(n\omega t + \varphi_{2n}) \\ +(\overline{V_{dc}} - \overline{V_{fly}}) \sum_{n=1}^{+\infty} G_{1n}\cos(n\omega t + \varphi_{1n}) \end{aligned} \tag{5}$$

Fig. 3 shows the switch gate states, switch voltages, and input filter voltage waveforms over one time period.

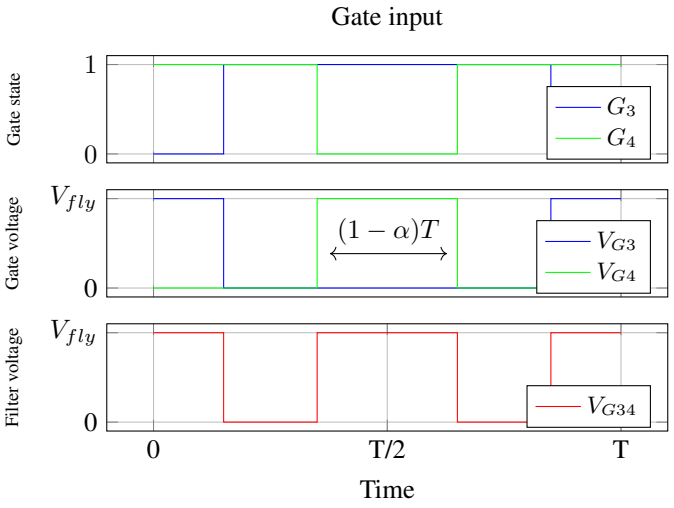

Figure 3. Input data generated by Switches

3.2. *Fuel Cell current ripple*

Expression (5) can be simplified due to the half voltage in the floating capacitor and the half-period delay. Additionally, using Fourier series, the ripple current study can focus on the AC part of the expression with the Fourier coefficient $\tilde{V}G34 = VG34(t) - \overline{V_{G34}}$ at twice the frequency $m = 2n$.

$$\tilde{V}_{G34}(t) = \frac{2V_{dc}}{\pi} \sum_{n=1}^{+\infty} \frac{\sin(m(1-\alpha)\pi)}{m}\cos(m\omega t) \tag{6}$$

For this study, ideal components are considered without internal resistances. The LCL filter transfer function shown in Fig. 1 can be described as:

$$H_{LCL}(s) = \frac{I_{L1}(s)}{V_{G34}(s)} = \frac{1}{L_1C_1L_2s^3 + (L_1+L_2)s} \tag{7}$$

Due to the transfer function, there is a resonant frequency that is a multiple of the switching frequency at:

$$\omega_{res} = \sqrt{\frac{L_1+L_2}{L_1C_1L_2}} = \frac{\omega}{K} \tag{8}$$

The purpose of this study is to reduce the fuel cell current ripple, which means we do not need to amplify any current harmonics. The first harmonic pulsation is at 2ω, so ideally $\omega_{res} << 2\omega$.

The filter current gain can be defined and applied to each frequency by (7)(8) as:

$$G_{LCL}(m\omega) = \frac{1}{m\omega(L_1+L_2)(m^2K^2-1)} \tag{9}$$

Using (9), it is possible to determine the resonant pulsation from which the first (and subsequent) harmonics are attenuated:

$$G_{LCL}(n=1) = 1 \implies K_{lim} = \sqrt{\frac{1+2\omega(L_1+L_2)}{8\omega(L_1+L_2)}} \tag{10}$$

This criterion can be used to adjust the resonant frequency value through the C_1 capacitor value.
The LCL filter argument must be considered because a delay should be added to the $\cos(n\omega t + \varphi_{LCL})$ terms. With ideal

components, $\varphi_{LCL} = 3\pi/2$. Therefore, the fuel cell AC current can be defined by (6)(9) as:

$$\tilde{I}_{L1}(t) = \frac{2V_{dc}}{\pi\omega(L_1+L_2)} \sum_{n=1}^{+\infty} \frac{\sin(m(1-\alpha)\pi)}{m^2(m^2K^2-1)} \sin(m\omega t) \quad (11)$$

The fuel cell current ripple can be studied from the previous expression (11). The peak current value is reached at $t = t_0$, which varies according to the duty cycle around $T/8$, as shown in Fig. 4.

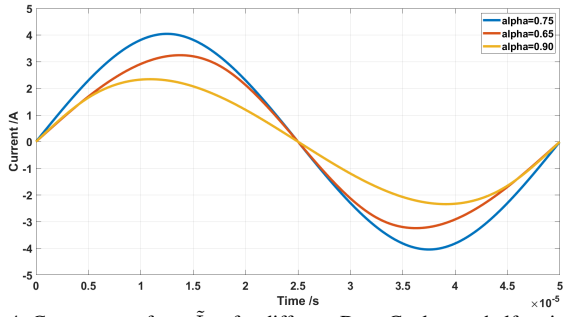

Figure 4. Current waveform $\tilde{I}_{L1}$ for different Duty Cycle on a half period

In order to determine the worst-case current ripple, $\tilde{I}_{L1}(t)$ has been plotted for several duty cycle values, as shown in Fig. 5.

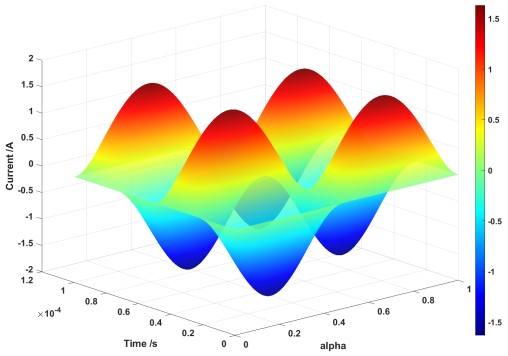

Figure 5. Current graph $\tilde{I}_{L1}$ for several duty cycle on a period

The maximum current value is reached at various times with different duty cycles. These conditions arise directly from the converter's multi-level architecture. The apparent frequency through the fuel cell inductor remains twice the switching frequency, and the maximum values are reached for the same duty cycle as a first-order L filter.

$$\Delta I_{L1} \leq \left\{ \begin{array}{l} 2\tilde{I}_{L1}\begin{pmatrix} t = 3T/8 \\ \alpha = 0.25 \end{pmatrix} \\ 2\tilde{I}_{L1}\begin{pmatrix} t = 7T/8 \\ \alpha = 0.25 \end{pmatrix} \\ 2\tilde{I}_{L1}\begin{pmatrix} t = T/8 \\ \alpha = 0.75 \end{pmatrix} \\ 2\tilde{I}_{L1}\begin{pmatrix} t = 5T/8 \\ \alpha = 0.75 \end{pmatrix} \end{array} \right\} \forall t \forall \alpha \quad (12)$$

Fuel cell current ripple constraints are provided by suppliers. These constraints could be a constant value corresponding to an aging test at a constant average current with a triangular or sinusoidal signal. Due to the third-order filter, the fuel cell current is closer to a sinusoidal waveform than a triangular one, as harmonic currents are well reduced.

For the subsequent parts of this study, we consider that $\Delta I_{L1} = 2\tilde{I}_{L1}(t = T/8, \alpha = 0.75)$. This consideration ensures that, in any case, the current ripple will be lower than the supplier's requirements. The ripple equations (12) and (11) are used to determine L_1, while L_2 remains unknown.

$$L_1 = \frac{4V_{dc}}{\pi\omega\Delta I_{L1}} \sum_{n=1}^{+\infty} \frac{\sin^2(m\pi/4)}{m^2(m^2K^2-1)} - L_2 \quad (13)$$

Expression (13) can result in a negative inductor value to achieve certain current ripple values. These conditions occur when the ΔI_{L1} requirement is too high or if the inductive value of L_2 is too large. There are several options to avoid these conditions. Firstly, accept a current ripple lower than the supplier's requirement. Secondly, reduce the frequency distance K between the switching and resonant frequencies by adjusting the C_1 capacitor value.

3.3. *Converter current ripple*

The current waveform through L_2 is designed to achieve a specific minimum current value. This minimum current value must be negative and less than a certain threshold current $\Delta I_{L2} = 2(\overline{I_{L2}} + I_{th})$, which is sufficient to charge the parasitic capacitors of the switching devices for ZVS switching, as shown in Fig. 6.

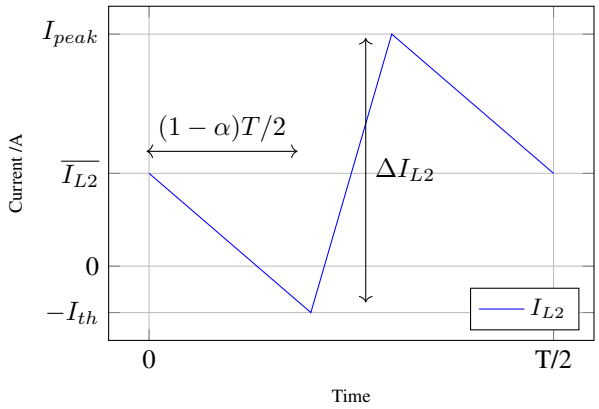

Figure 6. Current waveform example I_{L2} for Zero-Voltage-Switching

As previously mentioned for the LCL filter transfer function, it is possible to determine the current gain for each component:

$$\begin{array}{c} G_{L1}(m\omega) = 1/m\omega L_1 \\ G_{L2}(m\omega) = 1/m\omega L_2 \\ G_{C1}(m\omega) = m\omega C_1 \end{array} \quad (14)$$

There are two ways to determine I_{L2} with the same results. The first method involves using the voltage loop between V_{fc}, V_{L1}, V_{L2}, and V_{G34}. The second method involves using the voltage loop between V_{fc}, V_{L1}, V_{C1}, and the current node between I_{L1}, I_{C1}, and I_{L2}.

Current gain through each passive component is used for current/voltage conversion. The first method is chosen as an example to determine V_{L1} using (11) and (14).

$$\tilde{V}_{L1}(t) = \frac{-2V_{dc}L_1}{\pi(L_1+L_2)} \sum_{n=1}^{+\infty} \frac{\sin(m(1-\alpha)\pi)}{m(m^2K^2-1)} \cos(m\omega t) \quad (15)$$

Then $\tilde{V}_{L2}$ comes from voltage loop with (6) (15).

$$\tilde{V}_{L2}(t) = \frac{-2V_{dc}}{\pi}\sum_{n=1}^{+\infty}\frac{\sin(m(1-\alpha)\pi)}{m}\cos(m\omega t) + \frac{-2V_{dc}L1}{\pi(L1+L2)})\sum_{n=1}^{+\infty}\frac{\sin(m(1-\alpha)\pi)}{m(m^2K^2-1)}\cos(m\omega t) \quad (16)$$

Finally $\tilde{I}_{L2}$ is given by (14)(16).

$$\tilde{I}_{L2}(t) = \frac{-2V_{dc}}{\pi\omega L_2}\sum_{n=1}^{+\infty}\frac{\sin(m(1-\alpha)\pi)}{m^2}\sin(m\omega t) + \frac{-2V_{dc}L1}{\pi\omega L_2(L1+L2)}\sum_{n=1}^{+\infty}\frac{\sin(m(1-\alpha)\pi)}{m^2(m^2K^2-1)}\sin(m\omega t) \quad (17)$$

Using expression (17), it is possible to determine the current value I_{L2} at any time. The minimum value occurs at the switching time $t_1 = (1-\alpha)T/2$. To achieve ZVS conditions, the current value is defined as $\tilde{I}L2(t_1) = -\Delta IL2/2$, which allows us to derive expressions for L_1 and L_2:

$$\Delta I_{L2}/2 = \frac{2V_{dc}}{\pi\omega L_2}\sum_{n=1}^{+\infty}\frac{\sin^2(m(1-\alpha)\pi)}{m^2} + \frac{2V_{dc}L1}{\pi\omega L_2(L1+L2)})\sum_{n=1}^{+\infty}\frac{\sin^2(m(1-\alpha)\pi)}{m^2(m^2K^2-1)} \quad (18)$$

In the end, with expressions (13) and (18) depending only on L_1 and L_2, it is possible to determine the corresponding values for this application:

$$A = \frac{4V_{dc}}{\pi\omega\Delta I_{L1}}\sum_{n=1}^{+\infty}\frac{\sin^2(m\pi/4)}{m^2(m^2K^2-1)}$$

$$B = \frac{4V_{dc}}{\pi\omega\Delta I_{L2}}\sum_{n=1}^{+\infty}\frac{\sin^2(m(1-\alpha)\pi)}{m^2} \quad (19)$$

$$C = \frac{4V_{dc}}{\pi\omega\Delta I_{L2}}\sum_{n=1}^{+\infty}\frac{\sin^2(m(1-\alpha)\pi)}{m^2(m^2K^2-1)}$$

$$L2 = A(B+C)/(A+C)$$

$$L1 = A - L2$$

This current ripple design is feasible only if the converter operates far from functional points without ripple. Designing passive components with duty cycles around $\alpha = [0; 0.5; 1]$ will result in values close to zero for this type of converter architecture. This methodology is useful if the converter operates most of the time around $\alpha = [0.25; 0.75]$ at maximum power. In this case, the fuel cell current ripple requirements are met, and ZVS helps reduce switching losses at maximum power.

4. SIMULATION

4.1. LCL design

A real railway use case can be defined as shown in Table 1. It corresponds to the maximum fuel cell power functional point (high power, low voltage) and the maximum V_{dc} voltage during a battery recharge. For this point, the duty cycle is $\alpha = 0.7273$ and the average current is $I_{fc} = 400A$. With Fig. 4 and Fig. 5, the peak current is reached at $t = t_0 \neq T/8$, and (11) proves that t_0 depends only on α and K. Since the duty cycle is known, it is possible to determine t_0 by varying K. The ripple waveform is generated by the summation part in (11); only this part is displayed for several values of K in Fig. 7.

V_{fc}	300V
V_{dc}	1100V
Power	120kW
Ripple current	$\leq 10\%$
ZVS threshold current	5A
Architecture	3 levels Flying Capacitor
Switching frequency	10kHz

Table 1. Railway need specification

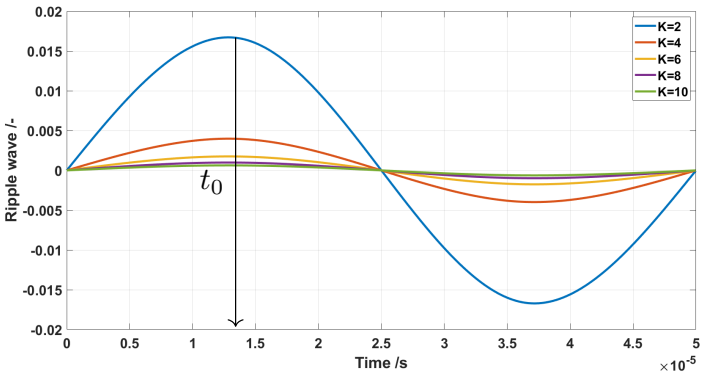

Figure 7. Ripple waveform on I_{L1} for several K at $\alpha = 0.7273$

Coefficient K won't change peak current time $t_0(\alpha = 0.7273) = 1.285e^{-5}s\ \forall K$.

$$L_1 = \frac{4V_{dc}}{\pi\omega\Delta I_{L1}}\sum_{n=1}^{+\infty}\frac{\sin(m(1-\alpha)\pi)}{m^2(m^2K^2-1)}\sin(m\omega t_0) - L_2 \quad (20)$$

$$L_1 = A_0 - L_2$$

Simply applying (20) and (19) will result in a negative inductance value for L_1. As previously described, rework is needed by either reducing the current ripple ΔI_{L1} or adjusting the coefficient K.

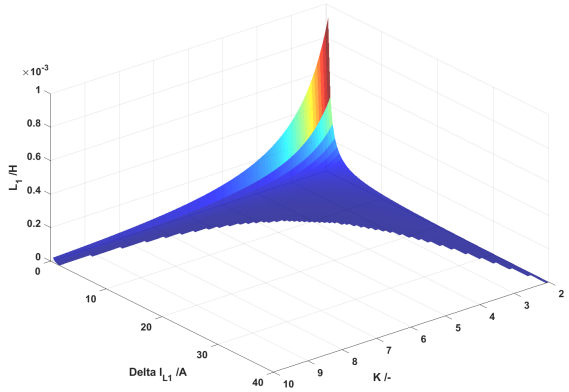

Figure 8. L_1 value function of K coefficient and ripple current ΔI_{L1}

Fig. 8 shows the variation of positive L_1 values as a function of the current ripple ΔI_{L1} or coefficient K, with negative values excluded. For the next part of this paper, we choose $K = \sqrt{10}$ and $\Delta I_{L1} = 8A$, as these values fall within the

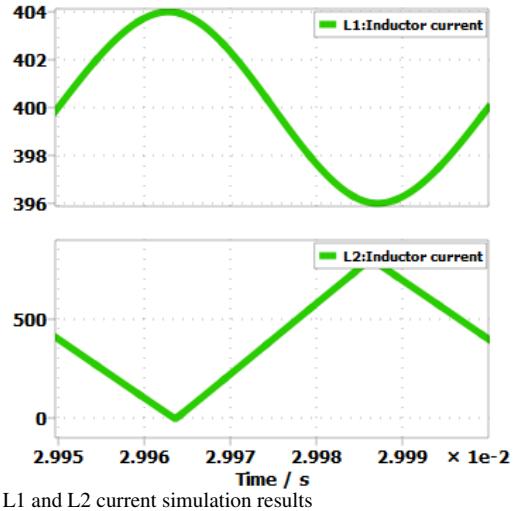

Figure 9. L1 and L2 current simulation results

authorized range. Finally, the LCL filter simulation is shown in Fig. 9 with $L_1 = 9.41\mu H$, $C_1 = 567\mu F$, and $L_2 = 8.51\mu H$. These components achieve the desired ripple current on the fuel cell side $\Delta I_{L1} = 8A$ and enable ZVS on the converter side $\Delta I_{L2} = 810A$. For comparison, the inductor value for the same fuel cell current ripple in the first-order case would be $L = 511\mu H$.

4.2. *Device losses*

Zero-Voltage Switching (ZVS) is used to reduce switching losses. At turn-on, the current through the devices is negative $I_{ON} = -5A$ and the voltage is still at the capacitor voltage $V_{ON} = 550V$. At this moment, the negative current allows the MOSFET to block, and the complementary body diode will be naturally triggered, sharing the current. There are no MOSFET switching losses thanks to this current sharing with the diode, resulting in $P_{ON} = 0W$.

At turn-off, the capacitor voltage remains the same as previously $V_{OFF} = 550V$, but the current is very high compared to classical switching, around the average value $I_{OFF} = 805A$. Therefore, P_{OFF} will be twice as high as without ZVS.

For example, a short comparison of switching losses can be made on an existing component "5SFG 0980B12000x" with and without ZVS, as shown in Table 2. To highlight the impact of

	No ZVS	ZVS
Temperature	150°C	
Frequency	10kHz	
Von = Voff	550V	
Ion	396A	-5A
Ioff	404A	805A
Eon	13.2mJ	0mJ
Eoff	5.8mJ	15.7mJ
Pswitch	190W	157W
Pcond	335W	462W
Ptot	525W	619W

Table 2. "5SFG 0980B12000x" losses comparison on the functional point

ZVS, we consider both cases with the same voltage, a switching frequency of $10kHz$, and the same junction temperature. The ZVS case is taken from the previous chapter, while the non-ZVS case is taken with $\Delta I_1 = 8A$, corresponding to a first-order inductive filter with the same filtering performance as the ZVS case.

As expected, switching losses are reduced by 17%, but total device losses increase by 18% in the ZVS case due to conduction losses. Total loss reduction would occur if we consider a fixed conduction drop voltage. However, according to device characteristics, this drop voltage depends on the current during conduction, increasing with high current and consequently raising conduction losses, as shown in Fig. 10.

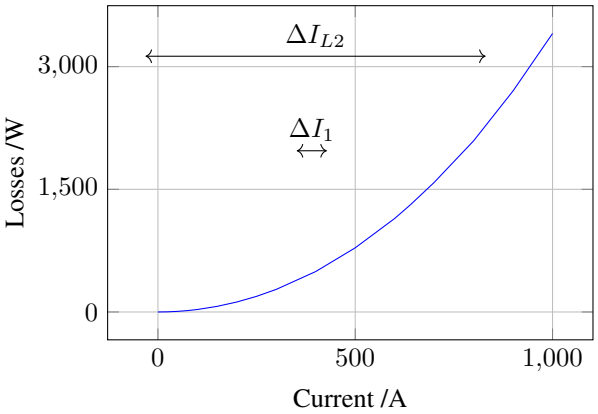

Figure 10. 5SFG 0980B12000x conduction losses characteristic at 150°C

In the end, switching losses are reduced by 33 W, while conduction losses increased by 127 W.

Even if Zero Voltage Switching (ZVS) does not reduce device losses, it is possible to achieve a different distribution of losses between conduction and switching. The characteristics of device losses are known, and the total device losses can be determined as a function of the current ripple for the required operating point.

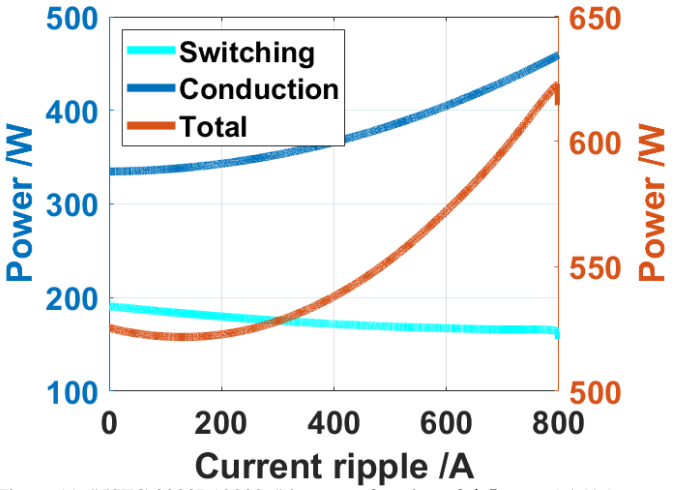

Figure 11. "5SFG 0980B12000x" losses as function of ΔI, $\alpha = 0.7273$, $F = 10kHz$, $I = 400A$

Figure 11 shows that the minimum losses for this device occur at $\Delta I_{opti} = 131A$ with losses amounting to 521 W. The gain in losses is not significant compared to low ripple current. Large ripple current is not beneficial for this operating point with this device.

To estimate the optimal ZVS application range, ΔI_{opti} can be calculated at various frequencies and average currents. The switching frequency ranges from 500 Hz to 50 kHz, and the average current ranges from 20 A to 500 A. For each point, ΔI_{opti} and efficiency are calculated using the following equation:

$$\text{Efficiency} = 100 \times \frac{\text{LossesNoRipple} - \text{LossesOptimalRipple}}{\text{Losses}_{\text{NoRipple}}} \tag{21}$$

This allows for the identification of where ZVS is useful and the associated loss reduction combined with an optimized current ripple, as shown in Figure 12.

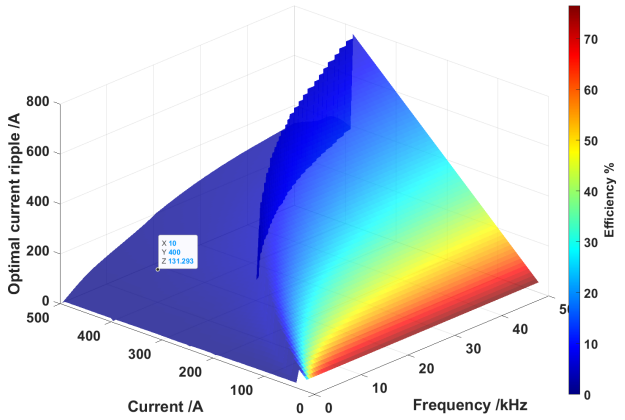

Figure 12. "5SFG 0980B12000x" losses gain at ΔI_{opti}, $\alpha = 0.7273$

This analysis demonstrates two distinct areas for ΔI_{opti}. On the left, the optimal ripple lies between ZVS and no ripple; our functional point (400 A and 10 kHz) falls within this area, where we observe a low efficiency of less than 10%. On the right, the optimal current ripple is at ZVS. Some points exhibit good efficiency, but this occurs at very low power. However, certain functional points are relevant at high frequencies, showing significant device loss reduction compared to the average current.

5. CONCLUSION

To conclude, this methodology can be used to design LCL filters for boost converter applications with high accuracy. The combination of ZVS and low Fuel Cell ripple current results in very low component values. This approach can also be applied to other converter architectures or types of filtering. A more accurate model could be developed by considering the internal resistance within passive components; however, this would make the Fourier series approach more complex with longer expressions.

While ZVS effectively reduces switching losses, this railway application demonstrates that ZVS does not reduce semiconductor losses. Due to the large current ripple range, conduction losses are too high and increase more than the decrease in switching losses. Device temperature stress will be higher, making it impossible to operate at higher frequencies. Even though the LCL component values are very small, high current ripple will stress C_1 and L_2. A capacitor of $567\mu F$ capable of supporting $810A$ peak-to-peak is uncommon. For L_2, this large current ripple will lead to increased iron losses in the magnetic component, potentially requiring a different inductor technology than L_1, especially to maintain the inductive value up to $805A$.

This approach is effective, but such an LCL filter with ZVS would be more beneficial in applications with lower average current and higher switching frequencies.

6. ACKNOWLEDGMENT

This project was funded by the French State in the frame of 2030 and Relaunch France, and by the European Union – NextGenerationEU.

7. REFERENCES

[1] O.Rallières, « Modélisation et caractérisation de Pile a Combustible et Electrolyseurs PEM », in Electrical Engineering, 14 Novembre 2011.

[2] Lluís Santolaria, «Comprehensive analysis of the impact of serial and parallel cooling on the thermal performances of power semiconductor modules », Hitachi ABB Power Grids, Switzerland, 7 May 2021.

[3] Athanasios Mesemanolis,, «Dynamic characteritics and SOA of the RoadPak SiC Module at multiple Operating Conditions», Hitachi Energy Switzerland Ltd, Switzerland, 12 May 2022.

[4] Young-Jung Kim, Hyosuung Kim «Optimal inductance ratio of LCL filter for grid connected inverters considering with low order harmonics», Kongju National University, October 2016.

[5] Carla Aparicida Felipe, Edivan Laercio Carvalho «Analytical methodoly to design third-order filter (LCL) for battery chargers», Universidad Tecnologica Federal do Paraña, Federal University of Santa Maria, February 2020.